Basic

Adaptive immunity

Research Article

Global k_{off}-rates of polyclonal T-cell populations merge subclonal avidities and predict functionality

Philipp Lückemeier[1], Katherine L. Molter[1], Sebastian Jarosch[1], Patrick Huppertz[1], Anna Purcarea[1], Manuel J. P. Effenberger[1], Magdalena Nauerth[1], Elvira D'Ippolito[1], Kilian Schober[#1,2] and Dirk H. Busch[#1] (ORCID)

[1] Institute for Medical Microbiology, Immunology and Hygiene, Technische Universität München (TUM), Munich, Germany

[2] Mikrobiologisches Institut–Klinische Mikrobiologie, Immunologie und Hygiene, Universitätsklinikum Erlangen, Friedrich-Alexander-Universität (FAU) Erlangen-Nürnberg, Erlangen, Germany

The avidity of TCRs for peptide-major histocompatibility complexes (pMHCs) is a governing factor in how T cells respond to antigen. TCR avidity is generally linked to T-cell functionality and there is growing evidence for distinct roles of low and high avidity T cells in different phases of immune responses. While physiological immune responses and many therapeutic T-cell products targeting infections or cancers consist of polyclonal T-cell populations with a wide range of individual avidities, the role of T-cell avidity is usually investigated only in monoclonal experimental settings. In this report, we induced polyclonal T-cell responses with a wide range of avidities toward a model epitope by altered peptide ligands, and benchmarked global avidity of physiological polyclonal populations by investigation of TCR-pMHC k_{off}-rates. We then investigated how varying sizes and avidities of monoclonal subpopulations translate into global k_{off}-rates. Global k_{off}-rates integrate subclonal avidities in a predictably weighted manner and robustly correlate with the functionality of murine polyclonal T-cell populations in vitro and in vivo. Surveying the full avidity spectrum is essential to accurately assess polyclonal immune responses and inform the design of polyclonal T-cell therapeutics.

📺 Additional supporting information may be found online in the Supporting Information section at the end of the article.

Introduction

CD8^{+} T cells are an integral part of the adaptive immune response. TCRs scan peptide–MHCs (pMHCs) of nucleated cells until sufficient binding occurs [1]. When primed, T cells proceed to kill target cells and secrete cytokines to protect them from intracellular pathogens and aberrant cells [2]. Despite being crucial to this process, our insight into the role of the TCR-pMHC binding strength—TCR avidity—is very limited.

High TCR avidity has been associated with many positive properties like functional avidity, pathogen clearance, and tumor

---

Correspondence: Dr. Kilian Schober and Dirk H. Busch
e-mail: Kilian.Schober@uk-erlangen.de; dirk.busch@tum.de

[#]These authors contributed equally: Kilian Schober, Dirk H. Busch

protection [3–5]. Low TCR avidity, on the other hand, still plays an important role in different phases of the immune response. Indeed, low avidity TCRs were shown to dominate the very early or late phases of the immune response, while high avidity T cells are either still being primed in the LN or have declined as a consequence of chronic antigen exposure [6–8]. Some evidence suggests an optimal avidity range for T-cell activation [9, 10]. Many factors influence TCR avidity. One of particular importance is the dissociation rate, or k_{off}-rate, of the TCR-pMHC complex [9]. Several assays have been developed to measure this parameter and have established a strong link with the properties mentioned above [5, 11–14]. However, these analyses usually require cell sorting or TCR isolation and re-expression. In fact, most studies assessing TCR avidity use clones, cell lines, and transgenic T-cell populations, or use crude parameters like average pMHC multimer binding capacity and the MFI reduction over time [15–17]. Therefore, not very much is known about the relevance of "global" structural TCR avidity values of polyclonal T-cell populations for predicting functionality. This is somehow surprising, as many T-cell therapeutics used in clinical settings like tumor infiltrating lymphocytes (TILs), virus-antigen-specific T-cell infusions, donor lymphocyte infusions (DLIs), or T cells responding to checkpoint inhibitors are generally polyclonal [18–21]. In a few studies, numerous single-cell clones have been generated to extrapolate their characteristics to the initial polyclonal population. These pioneering studies established first links between more complex TCR avidity repertoires and protective capacity [5], as well as TCR repertoire evolution [6], and demonstrate comprehensive correlations with functional readouts [22]. To more directly quantify the avidity of polyclonal T-cell populations, we previously developed a TCR-pMHC k_{off}-rate assay, with which it is also possible to analyze polyclonal populations ex vivo [23]. Whereas we have shown that this TCR-pMHC k_{off}-rate assay can provide highly accurate and reproducible measurements for monoclonal ex vivo cultured or in vitro engineered T cells, it has so far not been studied whether k_{off}-rate values derived from polyclonal T-cell populations integrate into robust parameters, for example, allowing predictions on functional qualities. We were particularly concerned about the possibility that rapidly dissociating pMHC complexes released by low avidity T cells—especially during the early measurement phase of the assay—could be caught by high affinity T cells and thereby bias the assay. However, published data indicate already that the relatively large distances between cells during the assay as well as rapid dilution of the probe make it unlikely that neighboring cells with different ligand binding capacities will significantly influence each other [23, 24]. These observations motivated us to investigate "global" TCR-pMHC k_{off}-rate values of ex vivo-derived polyclonal T-cell populations in more detail.

Here, we explored the utility and composition of this global parameter of structural TCR avidity to predict T-cell function at the population level. We demonstrated that we can robustly measure the k_{off}-rate of polyclonal CD8$^+$ T-cell populations responding to *Listeria* infection ex vivo. This global k_{off}-rate merges various subkinetics of individual clones in an unbiased

manner. We used an altered peptide ligand (APL)-based infection model to reliably induce polyclonal T-cell populations of similar phenotype, but significantly different global k_{off}-rates toward the model epitope OVA. This difference in structural avidity correlates well with the functional avidity and tumor killing capacity in vitro, as well as tumor protection in vivo. We further translated the method to human T-cell populations and found also here high predictability of global k_{off}-rates from constituent clones with known parameters.

Results

Measuring global k_{off}-rates of murine polyclonal T-cell populations

While TCR-pMHC k_{off}-rate measurements of monoclonal T-cell populations, such as SIINFEKL-specific T cells, have been extensively tested, dissociation kinetics of polyclonal populations remain obscure. Some studies have combined monoclonal dissociations of T cells sorted from the same polyclonal population to approximate global avidity [5, 22]. We aimed at directly measuring dissociation kinetics of polyclonal populations ex vivo on a flow cytometer without an intermediate sorting step by using our previously published methodology [23]. To do so, splenocytes were stained with a reversible and an irreversible pMHC multimers, resulting in double-multimer staining of antigen-specific, CD8$^+$ T cells (Fig. 1A). After baseline acquisition, d-biotin was added—without interrupting the analysis—to disrupt the reversible multimer and start the dissociation. The nonreversible multimer provided a steady signal to track antigen-specific T cells among nonspecific cells without sorting, while the reversible *Strep*-Tactin-APC backbone rapidly dissociated from the cell surface (Fig. 1B, C, E). The now monomeric, fluorescently labeled pMHCs dissociated from bound TCRs over time, enabling TCR-pMHC k_{off}-rate measurements of epitope-specific T cells via signal decay directly ex vivo (Fig. 1F). After establishing analyses of monoclonal populations, we were keen to apply this methodology to polyclonal T-cell populations. We infected C57BL/6 mice with *Listeria monocytogenes* (*L.m.*) expressing OVA, isolated the splenocytes 8 days after infection (d8 p.i.), and performed the same assay on T-cell populations binding to reversible and irreversible H-2K^b/OVA$_{257-264}$ (OVA MHC) multimers (Fig. 1G). We were consistently able to acquire dissociation kinetics of these infection-induced populations (Fig. 1H). We were curious to see whether we could acquire a global measure of the population's avidity. Thus, analogous to monoclonal populations, we fitted an exponential decay to the dissociations and measured what we termed global k_{off}-rates (Fig. 1H and J). To our surprise, we found that the half-lives spanned over a roughly ninefold range of values. To explore global k_{off}-rates of recall populations and find whether we could observe significant differences in avidity, we reinfected mice with *L.m.* OVA after 4 weeks of convalescence and performed the assay on the responding CD8$^+$ T cells (Fig. 1G and I). We measured a similar range of values with a nonsignificant
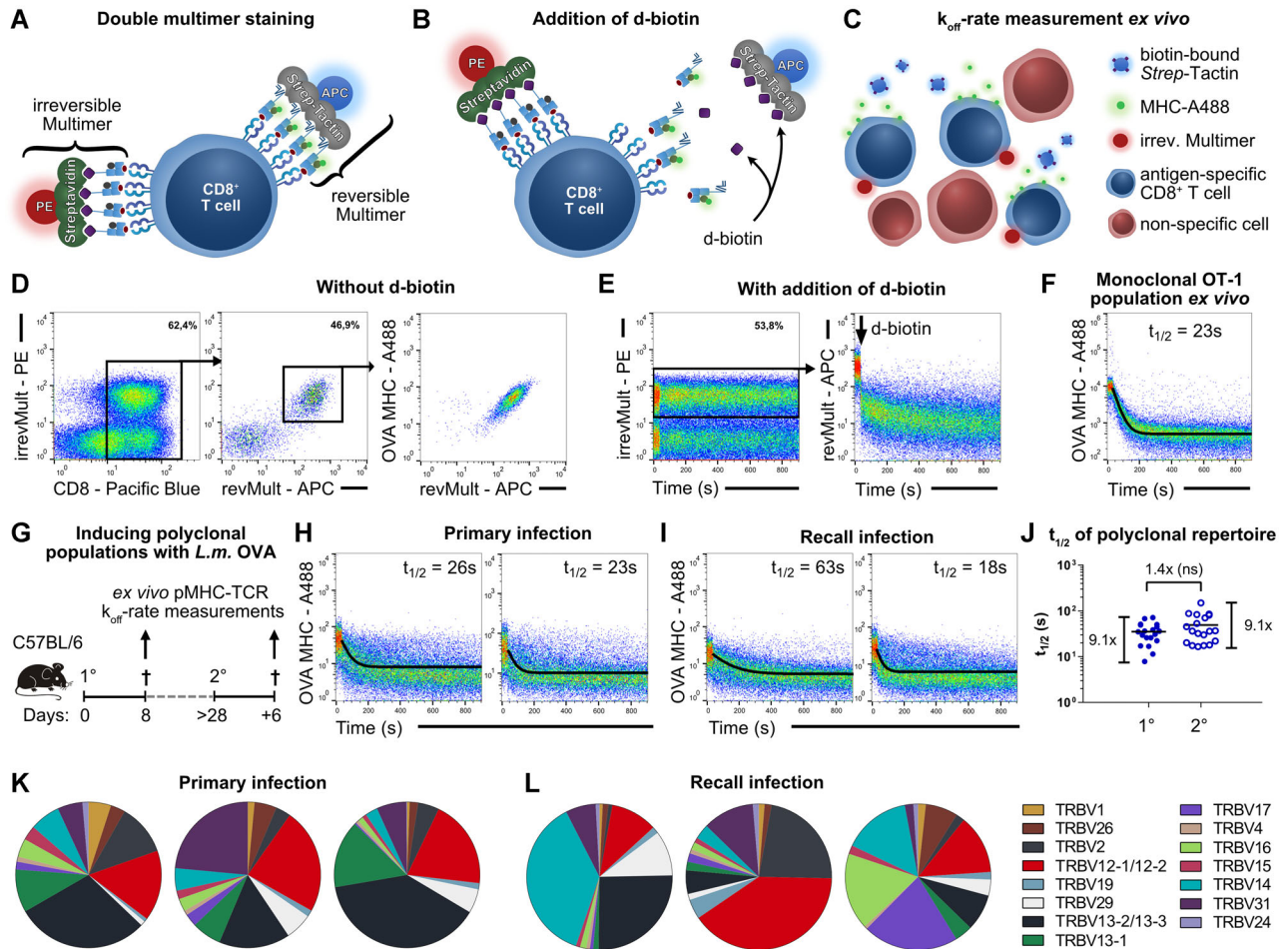
Figure 1. Measuring global koff-rates of murine polyclonal T-cell populations. (A, B, C) Schematic illustration of k_{off}-rate measurements ex vivo. CD8 molecules are omitted for simplicity. (A) Ex vivo samples get stained with biotinylated pMHC-streptavidin multimers (irreversible multimer) and strep-tagged pMHC-*Strep*-tactin multimers (reversible Multimer). Antigen-specific CD8$^+$ T cells bind both multimers. (B) Addition of D-biotin facilitates rapid dissociation of the *Strep*-tactin backbone and avidity-dependent dissociation of now monomeric pMHC molecules. (C) Antigen-specific CD8$^+$ T cells are distinguished from nonspecific cells ex vivo without prior sorting and despite signal loss of the reversible multimer via the irreversible multimer signal. (D, E) Gating strategy for TCR-pMHC k_{off}-rate measurements. Splenocytes were stained with aCD8, biotinylated H-2K^b/OVA$_{257-264}$ pMHC-streptavidin multimers (irrevMult) and strep-tagged H-2K^b/OVA$_{257-264}$ pMHC (OVA MHC)-*Strep*-tactin multimers (revMult). Purity of reversible multimer$^+$ events among irreversible multimer$^+$ events regularly exceeded 90%. € To track OVA-specific cells during dissociation, a gate was kept on irreversible multimer$^+$ cells while the reversible multimer rapidly dissociated after addition of D-biotin. (F) Representative plot of ex vivo monomeric OVA MHC dissociations and pMHC-TCR k_{off}-rate measurements of a monoclonal OT-1 population pregated as described in (D,E). (G) Experimental design. Mice were infected with *L.m.* OVA, sacrificed on d8 p.i. and H-2K^b/OVA$_{257-264}$-TCR k_{off}-rate measurements of splenocytes were taken. Alternatively, mice convalesced for over 4 weeks and received a recall infection with *L.m.* OVA thereafter. Measurements were performed on d6 after recall analogously to d8 p.i. (H, I) Representative monomeric OVA MHC dissociations and pMHC-TCR k_{off}-rate measurements of splenocytes described in (G), either on d8 p.i. (H) or d6 after recall infection (I). (J) Summary of $t_{1/2}$ of pMHC-TCR k_{off}-rate measurements of CD8$^+$ OVA multimer$^+$ splenocytes 8 days after primary (1°) and 6 days after recall infection (2°) with *L.m.* OVA. Each dot represents a mouse (n = 19 each from >10 independent experiments). Bars indicate means. There was a 1.4-fold increase in the average $t_{1/2}$ of polyclonal repertoires from 1° to 2° and 9.1-fold ranges between the lowest and highest $t_{1/2}$ in both infection settings. Unpaired t-test was performed between 1° and 2°. ns, not significant (p-value = 0.12). (K, L) Representative TRBV repertoires measured by flow cytometry showing polyclonality of CD8$^+$ OVA multimer$^+$ splenocytes 8 days p.i. (K) and 6 days after recall infection (L) with *L.m.* OVA. Each pie chart shows the repertoire of one mouse. Charts representative of two to three independent experiments with n = 2–3 mice each.

increase in the average half-life of the recall populations (Fig. 1J). To corroborate the polyclonal nature of these populations, we evaluated their T-cell receptor beta variable region (TRBV) repertoires (Fig. 1K and L). Indeed, we found widely varying TRBV frequencies between as well as broad spectra within immune responses, reflecting a certain variance between them and emphasizing their polyclonality. Overall, we could induce and

precisely measure k_{off}-rates of polyclonal antigen-specific TCR repertoires.

Global k_{off}-rates accurately merge subclonal avidities

Intrigued by the possibility to assess the structural avidity of the CD8$^+$ immune response against defined epitopes directly ex vivo,

we now aimed to better understand the composition of global k_{off}-rates. It was unclear whether subclonal avidities merge in an additive, multiplicative, or inconsistent manner and whether low and high avidities contribute equally toward the global avidity. We were especially concerned that, during dissociations, competition and rebinding of pMHCs among T cells of differing avidities within a population would confound measurements of polyclonal samples [25]. Moreover, inadequacies of the "one-phase exponential decay" model used to fit one dissociation curve to the multiple kinetics within a polyclonal population might confound parameter predictions based on monoclonal dissociations merged together.

To test how individual clones and their sizes and avidities influence the global k_{off}-rates of the larger, polyclonal population, we made use of a murine TCR library for H-2K^b/OVA$_{257-264}$ (Fig. 2A, TCR library described in ref. [6]). By overlaying previously acquired dissociation data of two transgenic monoclonal populations of similar size in silico, we simulated an oligoclonal population consisting only of two clonal subpopulations (Fig. 2B). We fitted an exponential decay to the merged data to determine its global k_{off}-rate and found that this half-life accurately matches the mean of the half-lives of the constituent monoclonal populations (Fig. 2B). Next, we merged the dissociation data of all the TCRs pairwise in the library shown in Fig. 2A and performed the same in silico analyses as described above. The resulting half-lives of the oligoclonal populations indeed correlated well with the frequency-weighted mean of the half-lives of the constituent monoclonal populations when all pairs were taken into account (Fig. 2C). By using the MFI at the start and the end of the dissociations of the monoclonal populations, thus, accounting for differences in initial staining intensity, the "measured" half-lives of the paired populations correlated even more closely and could be predicted by the equation described in Supporting information Fig. S1 (Fig. 2D). Next, we aimed to show that this finding also holds true for actual ex vivo measurements of oligoclonal populations. We isolated two distinct and equally large T-cell populations retrogenically expressing separate T-cell receptors from the library as well as congenic markers. We stained for the congenic markers, pooled the samples, and gated on the congenic markers to track the distinct populations during the dissociation and separately calculated their k_{off}-rates (Fig. 2E). Then, we ungated and calculated the k_{off}-rate of the resulting biclonal population. With both populations exhibiting equal frequencies and similar MFIs at the start and end of the dissociations, the global $t_{1/2}$ nicely approximated the mean of the two $t_{1/2}$ (Fig. 2E). We repeated this experiment with all TCRs from the library and pooled two populations of different sizes and MFIs ex vivo to measure the monoclonal and global k_{off}-rates. Using solely the dissociation parameters from the constituent subpopulations, we were able to predict the global k_{off}-rates of the biclonal populations over a wide range of $t_{1/2}$ with high fidelity (Fig. 2F). This predictability suggests that global k_{off}-rates accurately and equally merge high, medium, and low subclonal avidities to form a parameter of global structural avidity.

Inducing T-cell populations with varying global k_{off}-rates

To test whether global k_{off}-rates are predictive of functionality, we first needed to induce T-cell populations with consistently differing global k_{off}-rates. Particular APLs of the OT-1 receptor, which have just one change in the amino acid sequence of the OT-1 ligand SIINFEKL (OVA$_{257-264}$) and are called SAINFEKL (A2), SIYNFEKL (Y3), and SIIQFEKL (Q4), respectively, were previously shown to exhibit an affinity toward OT-1 in decreasing order from SIINFEKL > A2 > Y3 > Q4, when presented on H-2k^b [8]. We hypothesized that, in an infection setting, these APLs could conversely induce polyclonal, endogenous T-cell populations with a similarly tiered global structural avidity toward the OVA MHC (H-2K^b/SIINFEKL).

As a baseline, we used *L.m.* expressing OVA$_{257-264}$ to infect mice and induce H-2K^b/SIINFEKL-specific T-cell populations. Global k_{off}-rates of polyclonal T-cell responses were consistently measurable with OVA MHC (Fig. 1H, J and 3A, B). Next, we infected mice with *L.m.* expressing the APLs mentioned above and produced specific H-2K^b/APL (APL MHC) k_{off}-rate reagents for each APL. We found that all APL-expressing *L.m.*-induced specific T-cell populations of which we were able to measure global k_{off}-rates with their respective cognate APL MHC (Fig. 3A and B). Compellingly, the average global $t_{1/2}$ of the *L.m.* APL-induced populations measured with their cognate APL MHC did not differ significantly from the average global $t_{1/2}$ of the *L.m.* OVA-induced populations measured with the OVA MHC (Fig. 3D, left side). This implied that all *L.m.* APLs were immunogenic and able to elicit a CD8$^+$ T-cell response of comparable global structural avidity toward their respective epitope as *L.m.* OVA. To assess whether the induced T-cell populations differed in their global k_{off}-rates toward the OVA epitope, we performed k_{off}-rate measurements with OVA MHC also of all *L.m.* APL-induced populations. Strikingly, average global $t_{1/2}$ of the *L.m.* APL-induced populations toward OVA indeed differed significantly from that of *L.m.* OVA-induced populations and even followed the same order as described above for the APLs and OT-1 T cells (Fig. 3D, right side). Compared with the *L.m.* OVA-induced populations, *L.m.* A2 showed very similar values, but we measured consistently and significantly lower values for *L.m.* Y3. OVA MHC-specific frequencies and kinetics in the *L.m.* Q4-induced populations were so low and fast that accurate quantification of the global $t_{1/2}$ was not possible.

We next sought to assess this model upon recall infection. After convalescing for 4 weeks, mice were reinfected with the same *Listeria* strain they were initially infected with. The global $t_{1/2}$ measurements of recall responses exhibited the same trend as measurements after primary infection, corroborating the initial findings (Fig. 3C and E). Here, too, we observed a mild, but robust increase in the average half-life of the recall populations compared to the populations after primary infection (Supporting information Fig. S2A). *Listeria monocytogenes* APL-induced CD8$^+$ T-cell responses showed lower OVA MHC$^+$ frequencies than corresponding APL MHC$^+$ frequencies (Supporting information Fig.

A Dissociations from murine TCR library for H-2K^b/OVA$_{257-264}$
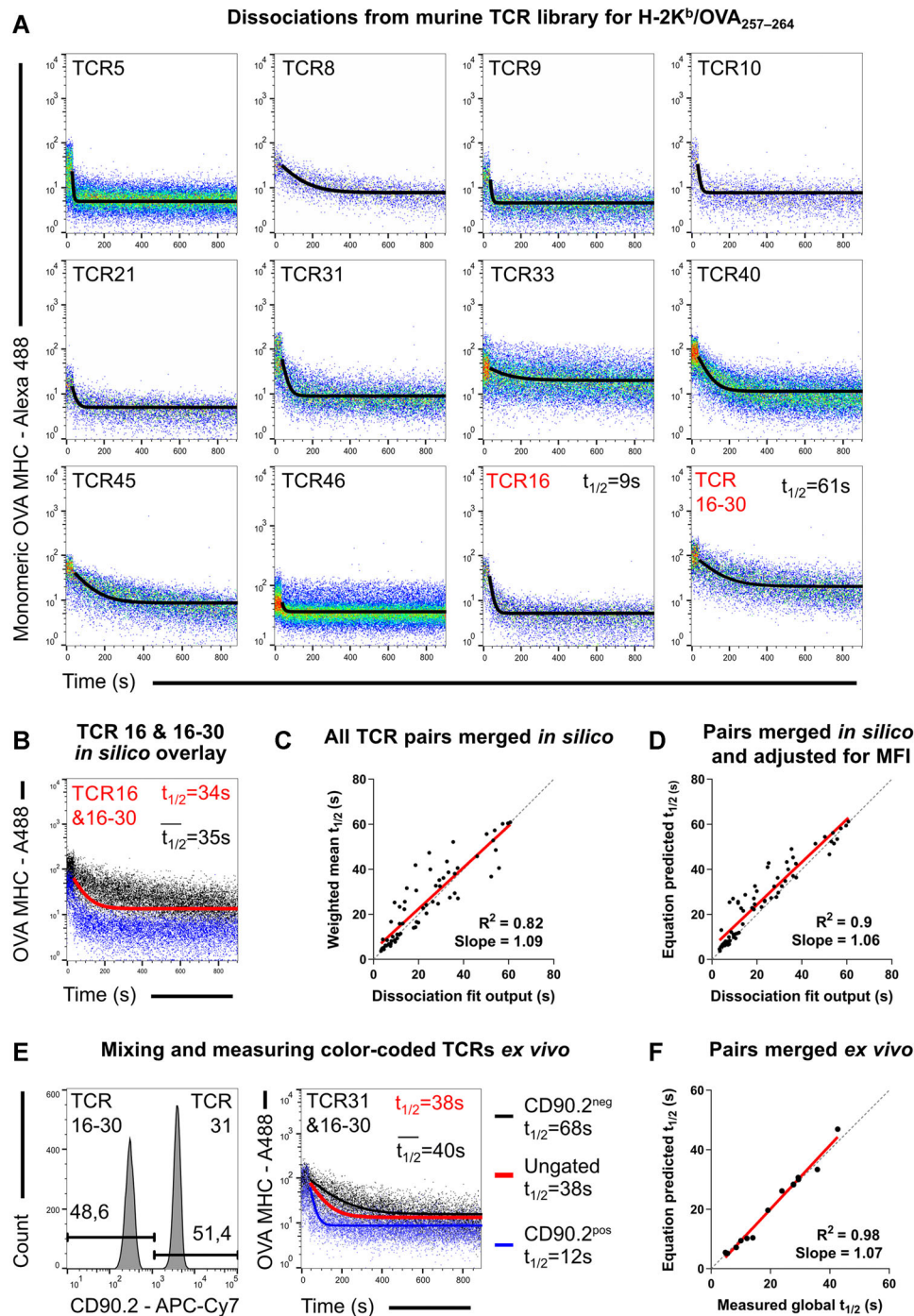

Figure 2. Global k_{off}-rates accurately merge subclonal avidities. (A) Representative monomeric OVA MHC dissociations from a TCR library for H-2K^b/OVA$_{257-264}$ described in Ref. [6]. (B) Overlay and exponential decay fit of the dissociations of two TCRs from separate measurements merged in silico. The t1/2 obtained from the fit is shown in red while the mathematical average t1/2 is shown in black. (C) All possible pairs of the shown dissociations of the TCRs were formed and merged in silico. Exponential decays were fitted to those merged dissociations and correlated with the weighted mean of their measured t1/2. (D) The merged dissociations and their fitting outputs described in (C) were correlated with an equation predicted t1/2. The equation only uses the weighted means of the t1/2 and the MFIs at the start and the end of the constituent dissociations as inputs and is described in more detail in Supporting information Fig. S1. (E) Exemplary plots of color coding, pooling, and simultaneously measuring H-2K^b/OVA$_{257-264}$-TCR k_{off}-rates of two T-cell populations each retrogenically expressing one of the TCRs shown in (A). The $t_{1/2}$ obtained from the fit is shown in red while the mathematical average $t_{1/2}$ is shown in black. For color codes, T cells were either stained with antibodies against congenic markers or not. Dissociation data of the mixed and single dissociations were extracted by gates on the respective color code. (F) Measured global $t_{1/2}$ of the dissociations described in (E) were correlated to predictions of global $t_{1/2}$ made with the equation described in (D) using the parameters of the singular dissociations as input. n = 15 dissociations of TCR pairs from six independent experiments. Red solid lines represent linear regressions. Grey dashed lines are graphs of f(x) = x.
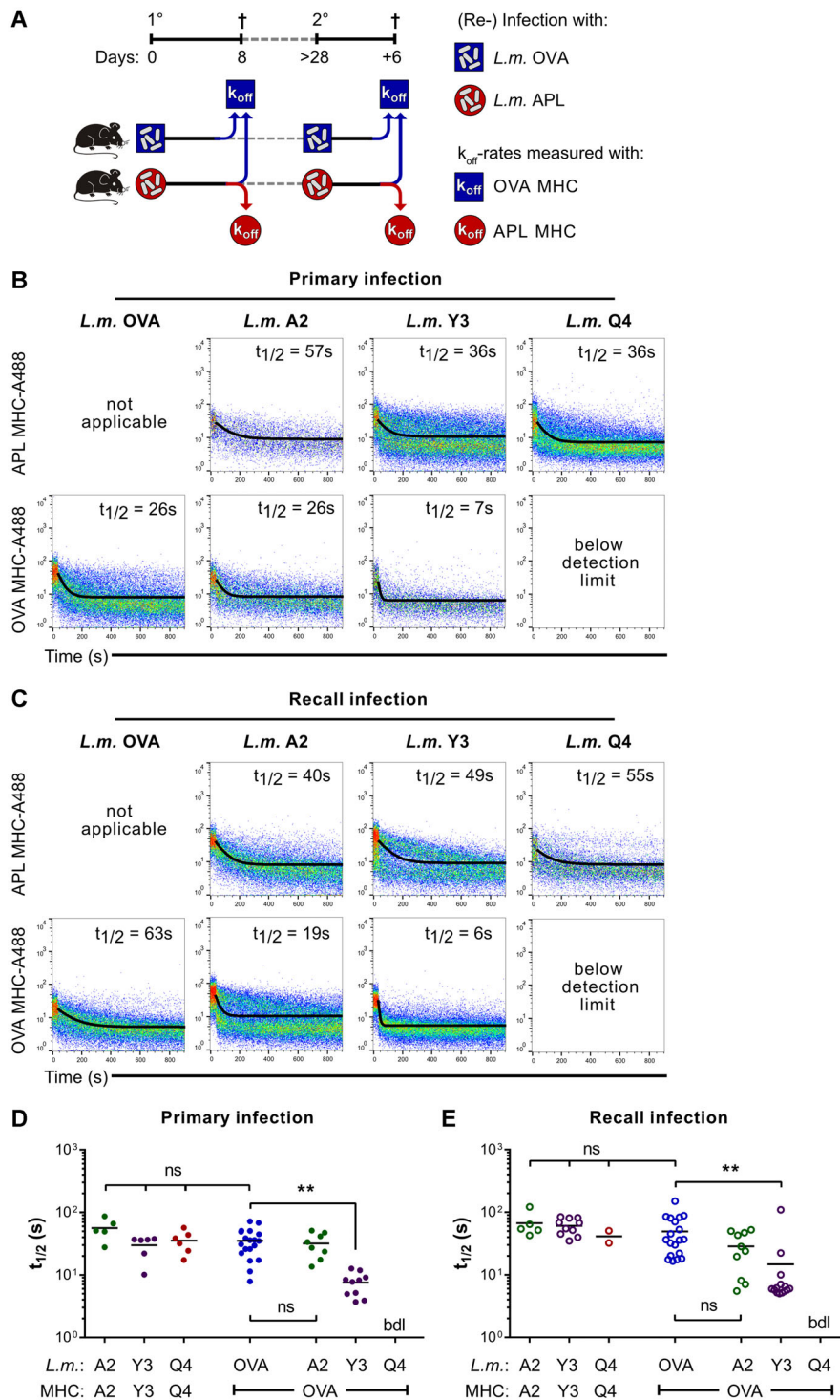
Figure 3. An APL-based *L.m.* infection model induces T-cell populations with consistently tiered global k_{off}-rates. (A) Experimental design. Mice were infected with *L.m.* OVA or *L.m.* expressing one of three altered peptide ligands (*L.m.* APL, A2/Y3/Q4). Mice were sacrificed on d8 p.i. and H-2K^b/OVA$_{257-264}$-TCR k_{off}-rate measurements of the splenocytes of both groups were taken. k_{off}-rate measurements of H-2K^b/APL-TCR were performed additionally on splenocytes of *L.m.* APL-infected mice. Alternatively, mice convalesced for over 4 weeks and received a recall infection with the initial pathogen thereafter. Measurements were performed on d6 after recall analogously to d8 p.i. (B, C) Representative pMHC-TCR k_{off}-rate measurements with cognate H-2K^b/APL (upper rows) or with foreign H-2K^b/OVA$_{257-264}$ (lower rows) on d8 p.i. (B) or d6 after recall infection (C). The inducing *Listeria* strain is indicated column-wise above the panels. *L.m.* Q4 infections induced T-cell populations with insufficient frequencies of H-2K^b/OVA$_{257-264}$ multimer binding cells. (D, E) Summary of pMHC-TCR k_{off}-rate measurements on d8 p.i. (D) or d6 after recall infection (E). The inducing *Listeria* strain is indicated in the upper, the pMHC used for pMHC-TCR k_{off}-rate measurements in the lower row. $n = 5$–19 (D) or $n = 2$–19 (E) from >10 independent experiments. Each dot represents a mouse. Bars indicate means. Ordinary one-way ANOVAs followed by Tukey tests were performed on the leftmost and rightmost four groups of each graph. **p-value < 0.01. ns, not significant; Bdl, below detection limit.

S2B and C). MHC$^+$ frequencies varied depending on the inducing *L.m.* strain and MHC used, while recall responses exhibited consistently higher frequencies regardless of the MHC used for staining. OVA Mult$^+$/APL Mult$^+$ ratios were surprisingly stable within groups (Supporting information Fig. S2D and E) and followed the order described above, arguing for robust induction of polyclonal populations with different avidities irrespective of individual TCR repertoires. We aimed to determine whether OVA MHC binding

cells were part of the APL-specific immune response and, thus, cross-reactive or whether they were recruited from a different pool. To avoid multimer competition, we sorted *L.m.* APL-induced splenocytes stained with cognate MHC streptamer, removed the staining reagent with d-biotin, and restained the sorted cells with OVA multimer (Supporting information Fig. S2F). These OVA Mult$^+$ frequencies were comparable to the OVA Mult$^+$/APL Mult$^+$ ratios measured before, confirming that OVA multimer-

binding subpopulations are indeed largely cross-reactive (Supporting information Fig. S2G). Only a minute amount of APL MHC$^-$ cells bound OVA MHC, suggesting that they barely contribute to the OVA MHC binding populations (Supporting information Fig. S2H). All infection settings induced polyclonal T-cell populations with diverse TCR repertoires under all MHC staining conditions (Supporting information Fig. S3A–D). In conclusion, we were able to induce polyclonal T-cell populations with robustly tiered global k_{off}-rates towards the OVA model epitope in primary and recall responses.

Global k_{off}-rates correlate well with functional avidity

In a next step, we aimed to correlate global k_{off}-rates as a measure of structural avidity to peptide sensitivity ("functional avidity"). We induced murine T-cell responses with the different *Listeria* strains as described in Fig. 2. First, we stimulated the splenocytes with increasing doses of the peptide which corresponded to the antigen expressed by the *Listeria* strain they were induced by (Fig. 4A and B, upper rows). The mean functional avidity did not significantly differ between the populations in any homologous infection setting, that is, when the cognate antigen was used (Fig. 4C and D). Second, we used the SIINFEKL peptide as a stimulus on all populations (Fig. 4A and B, lower rows). We observed a stark and highly significant difference in functional avidity toward SIINFEKL depending on the inducing *Listeria* strain (Fig. 4C and D). Importantly, the populations exhibited the same order as with the global k_{off}-rates (compare Fig. 3D, E and 4C andD). These differences in functionality could not be explained by differences in phenotypic compositions of the population, since all populations exhibited comparable and robust frequency distributions of effector, effector memory, and central memory subsets (Supporting information Fig. S4A and B). Similarly, the frequencies of multimer binding cells with a naïve phenotype were low in all infection and multimer staining settings (Supporting information Fig. S4C to E). To investigate the relationship of the global k_{off}-rate and functional avidity of a given population on a more granular level, we simultaneously performed both assays with equivalent epitopes and correlated the results. We found a significant positive correlation between the parameters in both primary and recall infection settings (Fig. 4E and F). We included seven different homologous and heterologous combinations of inducing epitopes and epitopes used in the respective assays (see Supporting information Fig. S5 for a more detailed view). Overall, these data demonstrated a strong link between the global k_{off}-rate and the functional avidity of polyclonal CD8$^+$ T-cell populations.

Global k_{off}-rates are predictive of in vitro and in vivo tumor killing capacity

Following these results, we aimed at assessing the populations' abilities to kill OVA-expressing tumor cells. First, we investigated the killing capacity in vitro by using PancOVA, an OVA-expressing

adherent tumor cell line, and the xCELLigence assay. To control for the number of OVA-specific CD8$^+$ T cells per group, we stained and sorted for OVA multimer$^+$ cells from populations induced by recall infections with *L.m.* OVA, *L.m.* A2, and *L.m.* Y3 (Fig. 5A). *Listeria monocytogenes* Q4-induced populations and the primary infection setting showed OVA multimer$^+$ frequencies that were too low to be included in this assay. We seeded out PancOVA cells and added the sorted T cells in different concentrations. We quantified the killing capacity (cytolysis) after 48 h (Fig. 5B). At both effector-to-target (E:T) cell ratios, the *L.m.* OVA and *L.m.* A2-induced T cells mediated a significantly higher killing capacity compared to *L.m.* Y3-induced T cells (Fig. 5C). These data reiterated the order described before. In parallel to this assay, we also measured the global k_{off}-rate of all populations before sorting with the OVA MHC. This enabled us to correlate tumor-killing capacities with the global k_{off}-rate of each population. We found a strong positive correlation between the two parameters reflecting the results acquired in the peptide sensitivity assays (Fig. 5D and 4E and F). We next went on to translate these in vitro findings to an in vivo model. Utilizing a model of OVA-expressing MC38-OVA tumor cells injected subcutaneously, we measured the tumor protection effect of transferred T cells by measuring the days until the tumor reached a critical size and mice had to be sacrificed (Fig. 5E). We irradiated recipient mice before tumor transfer to minimize the influence of an endogenous immune response and to also provide a favorable environment for transferred T cells. T cells were induced by a primary infection of the *Listeria* strains discussed earlier, sorted for CD8$^+$/OVA MHC$^+$, and were administered after recipient irradiation. The resulting survival curves differed significantly and showed a modest, but distinct separation between the mice who received *L.m.* OVA or *L.m.* A2-derived T cells and those who received *L.m.* Y3-derived T cells, or just saline solution as a negative control (Fig. 5F). In summary, the in vitro and in vivo tumor killing data substantiate the predictive capacity of global k_{off}-rates and their correlation with functionality.

Subclonal avidity mixtures predict global k_{off}-rates with high fidelity in humans

Finally, we wanted to validate global k_{off}-rates as a summarizing measure of structural avidity in polyclonal T-cell populations in humans. As previously performed for murine T cells (Fig. 2), we sought to thereby make use of a collection of monoclonal populations with the same specificity and a wide range of avidities to, when pooled, examine the connection of the emerging global k_{off}-rate and the constituent k_{off}-rates. To this end, we turned to a single-cell expansion of yellow fever virus vaccine (YFV)-induced memory T cells, as these have been shown to persist over a long time period and rapidly expand in vitro [26]. We sorted single naïve-like, double HLA-A2/YFV NS4B$_{214-222}$ (pHLA) multimer$^+$ CD8$^+$ T cells from a healthy vaccinated donor and expanded them in vitro (Fig. 6A). We wanted to imitate the conditions of measuring a polyclonal population and eliminate technical confounders as much as possible. To achieve this, we again
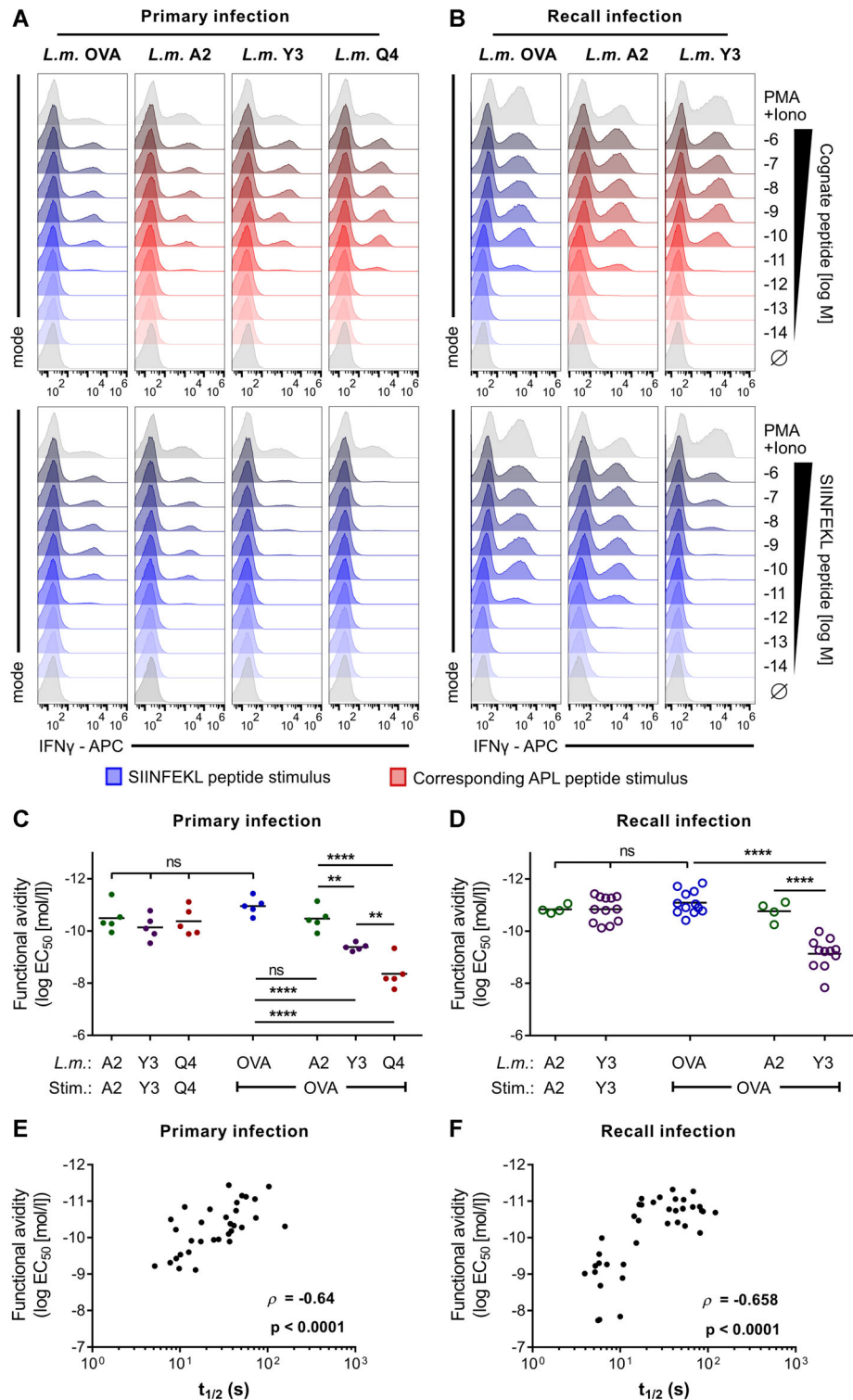
Figure 4. Global k_{off}-rates correlate well with functional avidity. (A, B) Peptide sensitivity. Representative plots of frequency of IFN-γ^+ of CD8$^+$ cells upon stimulation with increasing amounts of corresponding (upper rows) or SIINFEKL (lower rows) peptide, PMA + Ionomycin or no peptide (∅) on d8 p.i. (A) or d6 after recall infection (B). The inducing *Listeria* strain is indicated column-wise above the panels. Samples of *L.m.* OVA-induced populations are shown in upper and lower rows for better comparison. (C, D) Quantification of log EC$_{50}$s of IFN-γ release upon peptide stimulation (functional avidity) on d8 p.i. (C) or d6 after recall infection (D). The inducing *Listeria* strain is indicated in the upper, the peptide used as stimulus in the lower row. n = 4–12 from eight independent experiments. Each dot represents the spleen of a mouse. Bars indicate means. Ordinary one-way ANOVAs followed by Tukey tests were performed on the leftmost and rightmost four (C) or three (D) groups of each graph. *p*-values: ** < 0.01, **** < 0.0001. ns, not significant. (E, F) Correlation of simultaneous pMHC-TCR k_{off}-rate and peptide sensitivity measurements where corresponding epitopes were used in both assays on d8 p.i. (E) or d6 after recall infection (F). n = 32–38. Each dot represents a mouse. Spearman correlation.

utilized color codes by giving each colony a unique fluorochrome combination to be able to pool several colonies in one sample. After 9 days of expansion, we labeled individual colonies with a unique color code, pooled them into one sample, measured the pHLA-TCR k_{off}-rate, and decoded respective colonies in silico according to their color code (Fig. 6B). We included 12

large, monoclonal dissociations for further analysis. The clones spanned a wide range of sizes and $t_{1/2}$ values (Fig. 6C and Supporting information Fig. S6A). We gated on clone b and clone k with varying $t_{1/2}$, but similar sizes of 2675 and 2308 events, respectively (Fig. 6D and Supporting information Fig. S6B), to obtain a pHLA-TCR dissociation of a defined, composite human
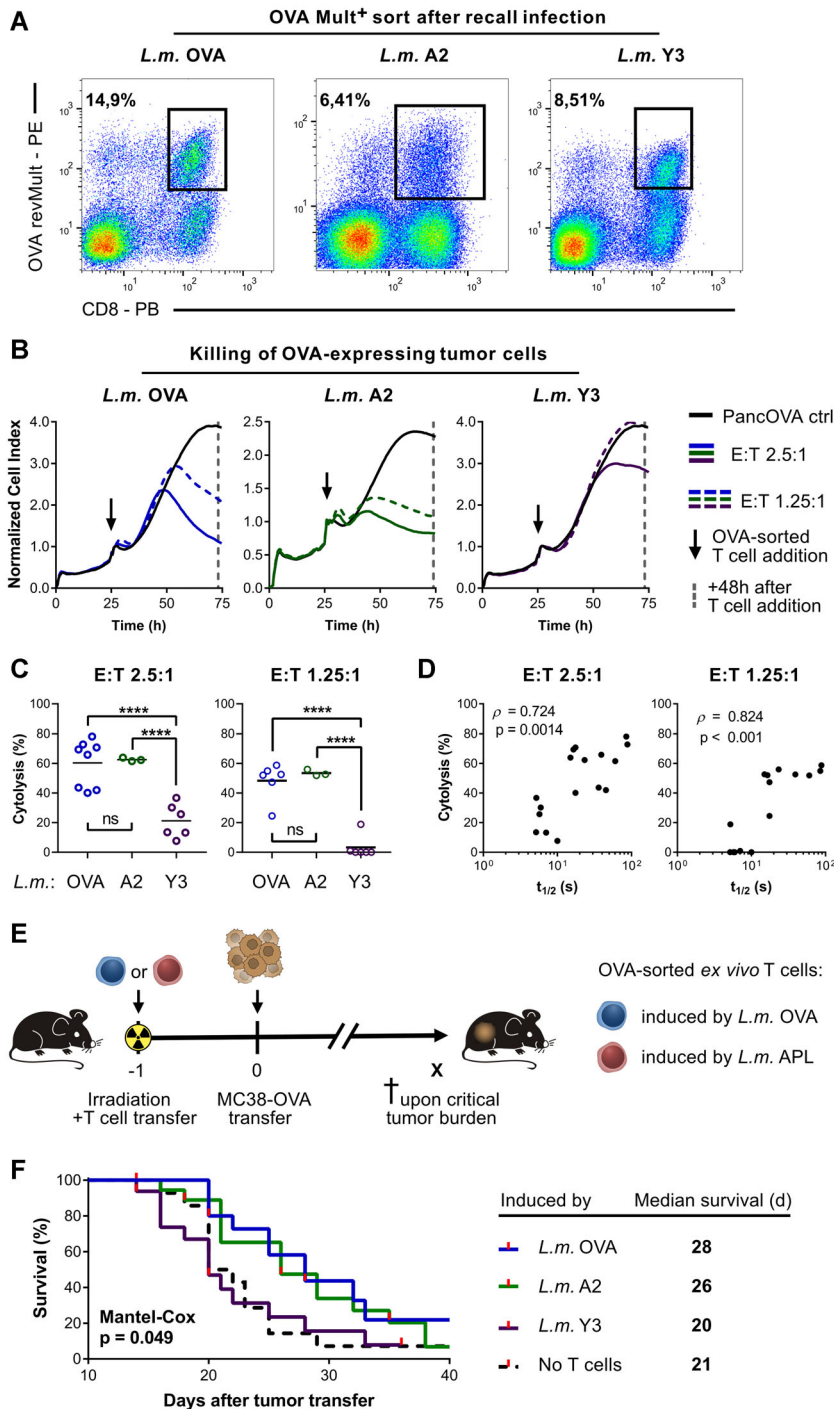
Figure 5. Global k_{off}-rates are predictive of tumor killing capacity in vitro and in vivo. (A) Representative plots of fluorescence associated cell sorting of CD8^{+}, reversible OVA multimer^{+} populations for tumor killing assays on d6 after recall infection. Multimer staining was reversed with D-biotin before T-cell transfer. Inducing *Listeria* strains are indicated above the plots. (B) Representative plots of real-time tumor killing assays. OVA expressing tumor cells (PancOVA) were grown for 24 h before either the populations described in A or medium alone were added (indicated by arrows) in different effector to target ratios (E:T). Cell indices were normalized to those time points, and the difference between wells with and without T cells 48 h later measured as cytolysis in %. Lines represent means of at least three wells. (C) Quantification of cytolysis at different E:T. Inducing *Listeria* strains are indicated below graphs. n = 3–8 from four independent experiments. Each dot represents a mouse. Bars indicate means. Statistics: Ordinary one-way ANOVAs followed by Tukey tests. ****p-value < 0.0001. ns not significant. (D) Correlation of simultaneous pMHC-TCR k_{off}-rate and cytolysis measurements at different E:T (upper and lower panel) on d6 after recall infection. n = 15–17 per E:T ratio. Each dot represents a mouse. Spearman correlation. (E) Experimental design. CD8^{+}, reversible OVA multimer^{+} populations were sorted from spleens on d8 p.i. with either *L.m.* OVA or *L.m.* APL. Recipient mice were irradiated, and sorted populations transferred 1 day before OVA-expressing tumor cells (MC38-OVA) were injected into the flank. Mice were monitored and sacrificed upon critical tumor burden. (F) Left: Kaplan–Meier survival plot of mice specified in (E). Recipients were grouped by *Listeria* strains that induced the sorted populations they received. Right: Legend and table of median survival in days after MC38-OVA transfer. n = 15–19 per group. Mantel-Cox log rank test for all-curve difference.

biclonal T-cell population. Its measured global $t_{1/2}$ was 145 s, approximating the 147.5 s mean $t_{1/2}$ of clone b and clone k when weighted 1:1 (Fig. 6D). When adjusted for size, the global $t_{1/2}$ of all biclonal populations possible to construct from the 12 clones was accurately predicted by the previously mentioned equation, as seen before for murine T cells (compare Fig. 6E and 2D, F and Supporting information Fig. S1). These findings underpin that human as well as murine global k_{off}-rates linearly, equally, and accurately merge subclonal k_{off}-rates in a size-weighted manner.

Based on that premise, we were curious to which degree of fidelity our equation could predict global k_{off}-rates, given that all subclonal dissociation parameters are known. We generated 1000 artificial polyclonal population dissociations consisting of all 12 clones mixed at random weights. The minimum frequency of a clone in the global population was 5% and the maximum was 50%. We first fed the three parameters—weights, MFIs, and subclonal k_{off}-rates—for each artificial population into the equation to predict the global k_{off}-rate. Then, we acquired the actual global
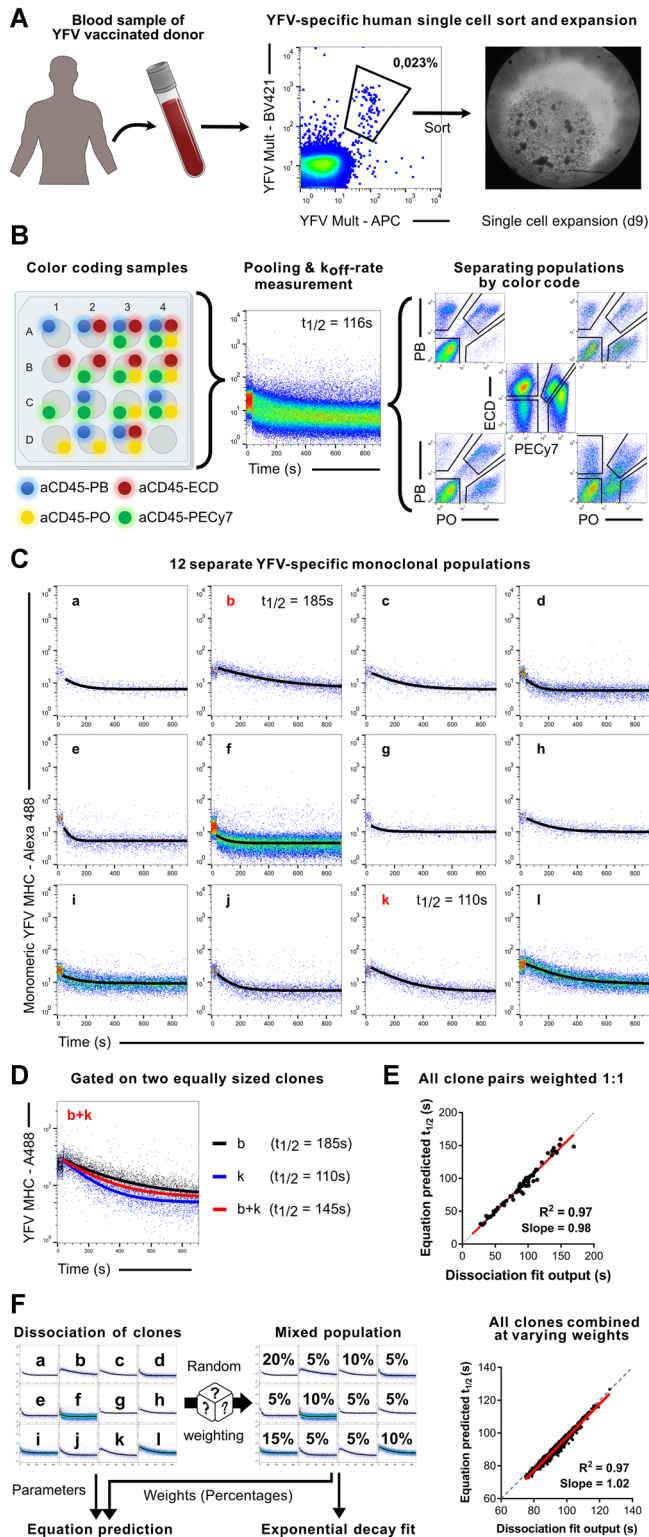
Figure 6. Global k_{off}-rates can be predicted with high fidelity from subclonal avidity mixture in humans. (A) Overview of single cell isolation and expansion. PBMCs of a yellow fever virus (YFV) vaccinated human donor were isolated from a blood sample and stained. PI$^-$, CD19$^-$, CD8$^+$, CCR7$^+$, CD45RA$^+$, double HLA-A2/YFV NS4B$_{214-222}$ multimer$^+$ (YFV-specific) single cells were sorted into a microtiter plate and expanded in a feeder-free cell culture. (B) Expanded populations originating from the single cells described in (A) were restained at day

k_{off}-rate by computationally fitting an exponential decay to the flow cytometry data and the weights (Fig. 6F). The predictions very closely matched the global $t_{1/2}$ outputted by the exponential decay fit. This suggested that the global k_{off}-rate of polyclonal T-cell populations with up to a dozen or more subclones of varying frequencies can be predicted with high fidelity from the dissociation parameters of individual constituent clones, implying that carefully selected, previously characterized clones can be used to tailor the TCR avidity of polyclonal T-cell products.

Discussion

Here we explore, define, and validate the global TCR-pMHC k_{off}-rate as a measure for the structural avidity of polyclonal CD8$^+$ T-cell populations. Structural avidity of polyclonal populations correlates well with functional avidity, tumor killing capacity in vitro, and protectivity from tumors in vivo. Although the importance of TCR avidity in immune responses has been highlighted in numerous previous studies, the utilized T-cell populations have almost exclusively been monoclonal, genetically modified, or cell lines [3, 5, 22, 27, 28]. This limitation is likely rooted in technical shortcomings. Despite an abundance of TCR-pMHC avidity assays that demonstrate convincing correlations with functional parameters, most methods require cell sorting, cell culture, or even TCR isolation and re-expression [11, 13, 22, 24]. This invites selection bias, is resource-intensive, and might not be representative of the initial starting population. To assess the TCR avidity of polyclonal T-cell populations ex vivo, most research groups resort to pMHC multimer k_{off}-rate and/or staining intensity. Some studies do find a correlation of these parameters with functionality [3, 15, 16], while others do not [4, 29–32]. The value of these techniques has, therefore, remained ambiguous, obstructing a clear assessment of the properties and functional relevance of TCR avidity on a population level.

In this study, we used a large number of physiological murine T-cell populations in different infection settings and functionality

---

11 with aCD8, reversible YFV multimers, and each population stained with a unique combination of aCD45-fluorophore conjugates. All populations were mixed and read in as one sample to eliminate sample-to-sample variation. During analysis, the clones were identified via fluorophore combination and their pHLA-TCR k_{off}-rates calculated. (C) pHLA-TCR k_{off}-rates of 12 separate YFV-specific monoclonal populations obtained as described in (A) and (B). A table showing the size and $t_{1/2}$ of every population can be viewed in the Supplementaries. (D) Exponential decay fits of the approximately equally sized clones b and k in addition to that of both clones merged into one population. (E, F) Correlation between the $t_{1/2}$ fitted to the resulting dissociation curve after merging the given clones and of the $t_{1/2}$ predicted using only the means of their exponential decay parameters. (E) Two clones merged at a time after adjusting their size 1:1. (F) All 12 clones merged at varying weights. Left panel: schematic. The clones were assigned random weights of as little as 5% and as much as 50% and mixed into global populations. Right panel: Depiction of 1000 randomly chosen global populations. Each black dot represents one global population. Red solid lines represent linear regressions. Grey dashed lines are graphs of f(x) = x. One independent experiment is depicted. Another independent experiment is shown in Supporting information Fig. S7.

assays to examine the connection between polyclonal TCR-ligand avidity and functionality. This was enabled by the ex vivo applicability of our assay to pMHC multimer-binding T-cell populations [23]. As a limiting factor, T cells that would respond to antigen, but do not bind pMHC multimers, are imperceptible for our assay. Assuming most of them have a low structural avidity, this might lead to a slight overestimation of global avidity [33]. To reliably induce comparable T-cell populations with differing avidity, we utilized the established OVA-APL system to induce T-cell responses with different avidities toward the cognate epitope (the APL) and OVA. Remarkably, the avidity of these polyclonal populations toward OVA robustly depends on the inducing APL in a tiering reminiscent of the OT-1 TCR's avidity toward the APLs [8]. These data suggest that certain features of cross-reactivity determined in OT-1 T cells are representative for OVA-specific T cells in general, despite the vast interindividual diversity of the latter.

This conceptual validation indicates that our more physiological setup may prove instrumental in studying differences in TCR-ligand avidity of polyclonal populations.

In these polyclonal populations, we examined both structural and functional avidity simultaneously to study their relationship. Highly functional populations in vitro and in vivo tended to exhibit higher avidities toward their respective epitopes (Fig. 4 and 5). We also observed a slight and robust (albeit mostly statistically nonsignificant) increase in avidity from primary to secondary immunization (Supporting information Fig. S2A). This is in line with the previously reported "avidity maturation" of polyclonal T- cell populations upon recall responses [17, 34], although in our experimental setting, the extend of avidity maturation was only moderate. Interestingly, our data hint at a plateau in the correlation between global k_{off}-rate and functionality (Fig. 4 and 5). Similar findings have also been described for monoclonal populations [3, 35, 36].

We surveyed a wide range of avidities and found that slow and fast kinetics are integrated into global k_{off}-rates equally, without a bias for any level of avidity (Fig. 2). We initially were concerned about interactions between T cells of differing avidity within a sample, which would make measurements of polyclonal populations inherently error prone. Furthermore, we were uncertain whether fitting a single $t_{1/2}$ to a polyclonal dissociation could accurately reflect the global avidity. However, when pooled, constituent clones contribute linearly to a population's global avidity according to their frequency in mice and humans (Fig. 2 and 6). This excludes major interferences between subclonal populations during measurements and reveals the $t_{1/2}$ of polyclonal dissociations to be the frequency-weighted sum of constituent monoclonal dissociations. It also implies that high-avidity polyclonal populations are either exclusively composed of high-avidity subpopulations, or those of low avidity are counterbalanced by very high-avidity ones. While we were able to precisely merge subkinetics of individual clones into a global parameter of avidity, a vice versa dissection of the avidity composition for a polyclonal population is not possible. Some dissociations exhibit distinct "bands" with several monomorphic kinetics (Fig. 3C). However, these appear to be rare and confined to the recall infection setting, putatively

because of "avidity maturation." In general, a large spread of the dissociation pattern seems to hint at polyclonality and polyavidity (compare Fig. 2A and E), but we have not been able to utilize this as a robust parameter. The development of technologies to assess TCR avidity directly ex vivo on the single-cell level will provide novel technical solutions to address these questions.

In this study, we report how constituent clonal avidities compose a population's global avidity, and that global k_{off}-rates provide an important qualitative parameter for polyclonal T-cell populations, which might correlate with T-cell functionality in many settings. Insight into the composition of avidities could prove invaluable especially for immunotherapies utilizing polyclonal T-cell populations, like immune checkpoint inhibitors or cell infusions such as TILs, DLIs, and virus-specific T cells. Indeed, global avidity measurements could drive the selection of appropriate allogeneic donors for the adoptive transfer of highly functional virus-specific T cells. Similarly, as circulating T cells reflect the TCR repertoire of TILs in some extent [37], it might be feasible to identify cancer patients with pre-existing high-avidity antitumor T-cell immunity who, thereby, may benefit from TILs or checkpoint inhibitors therapies. With a growing understanding that T cells with differing TCR avidity take different roles in immune responses, mixing populations with high and low avidities might prove advantageous for epitope-specific T-cell therapy [38]. Pooling subpopulations of known global k_{off}-rates result in a population with a robustly predictable global k_{off}-rate. This property might aid in tailoring the avidity level of polyclonal cell products.

Materials and methods

Mice, infections, and cells

Six- to eight-week-old, female C57BL/6 inbred mice were purchased from Envigo and i.v. infected with 5×10^3 colony forming units of varying strains of *L.m.* The strains expressed recombinant OVA containing SIINFEKL (OVA$_{257-264}$) or containing the APLs SAINFEKL (A2, alanine substitute), SIYNFEKL (Y3, tyrosine substitute), or SIIQFEKL (Q4, glutamine substitute), as previously described [8]. Spleens were harvested on day 8 of the infection, mashed through a cell strainer, lysed with ACT for 7 min, suspended in standard FACS buffer (1× PBS, 0.5% w/v BSA, pH 7.45) and an aliquot counted in a Neubauer chamber with Trypan blue solution. Alternatively, mice were reinfected with the same *L.m.* strain over 28 days after the primary infection, and spleens were harvested, and prepared 6 days later as described above. Cells were used fresh. All animal experiments were approved by the District Government of Upper Bavaria (Department 5, Environment, Health and Consumer Protection). For human blood samples, written informed consent was obtained from the donors and use of the blood samples was approved according to national law by the local Institutional Review Board (Ethikkommission der Medizinischen Fakultät der Technischen Universität München).

Generation of pMHC molecules

pMHCs were generated as previously described [5]. In brief, H-2k^b and HLA-A*02:01 molecules with either a biotinylation substrate sequence for nonreversible multimers or *Strep*-tag residues for reversible multimers were refolded with either human or murine β2-microglobulin and a peptide. All pMHCs carry an artificially introduced cysteine residue (murine pMHCs at position 67 of the murine mβ2m, human pMHCs at a glycine serine linker by the *Strep*-tag). Murine pMHCs were refolded with either the SIINFEKL, A2, Y3, or Q4 peptides. Human pMHCs were refolded with either the LLWNGPMAV (YFV, NS4B) or the NLVPMVATV (CMV, pp65) peptides (synthesized by and purchased from Peptides and Elephants). *Strep*-tagged pMHCs were then conjugated with activated Alexa Fluor 488-maleimide dye (Thermo Fisher Scientific) at the cysteine residues. pMHCs with the biotinylation substrate sequence were biotinylated with a biotin-protein ligase. The refolded pMHCs were purified by size exclusion chromatography and stored in −80°C.

Flow cytometry

Samples were read in on a CyAn ADP 9 color (Beckman Coulter) or Cytoflex S flow cytometer (Beckman Coulter). Data were analyzed in FlowJo (FlowJo LLC) and Prism 7 (GraphPad Software, Inc.). Analyses adhere to the "Guidelines for the use of flow cytometry and cell sorting in immunological studies" [39]. A representative gating scheme for the first three gates (lymphocytes, singlets, living) used in all analyses can be viewed in Supporting information Fig. S7. Assays are MIATA compliant.

TCR-ligand k_{off}-rate assay

k_{off}-rate assays were performed as previously described [23]. In brief, nonreversible multimers were generated by adding 1 μg of biotinylated pMHC to 0.625 μg of streptavidin PE (Biolegend) and incubated in standard FACS buffer for at least 30 min. Reversible multimers were generated by adding 1 μg of *Strep*-tagged and fluorophore-conjugated pMHCs to 1 "test volume" of Strep-Tactin APC, as specified by the supplier (IBA Lifesciences), and incubated in standard FACS buffer for at least 30 min. A total of 5×10^6 splenocytes were resuspended in the reversible multimer solution for at least 45 min. CD8a (Pacific Blue, Life Technologies, clone 5H10-1) and CD19 (PE-CF594, BD Biosciences) antibodies were added after 25 min and coincubated for at least 20 min. Cells were washed and resuspended in a nonreversible multimer solution of the same specificity as the reversible multimers as well as 0.2 μg of PI for exactly 10 min. Cells were then washed, placed in FACS tubes held in a cooling device (qutools GmbH, Munich, Germany) to keep the temperature at 5.5°C and read in. After 30 s, 1 mL of a 2 mM D-biotin solution was added without interrupting the sample flow to initiate the dissociation. Samples were analyzed for 15 min. The acquired live, CD19$^-$,

CD8$^+$, nonreversible multimer$^+$ events were analyzed in FlowJo and exported to a custom application that determined the exact start time of the dissociation based on the stark drop in *Strep*-Tactin APC MFI after the addition of d-biotin. Data points were then imported into Prism 7, and the k_{off}-rates of the TCR-pMHC dissociation were calculated using a one-phase exponential decay model with the pMHC MFI from before the addition of d-biotin set as *Y0* value.

Phenotype and TRBV staining

Splenocytes were isolated as described above. Suspensions were split into 15 samples, incubated with Fc-block (BD Bioscience) and 0.1 μg Ethidium-monazide-bromide (EMA, Molecular Probes) for 20 min under light, washed, stained with respective nonreversible multimers, and incubated for 45 min. After 25 min, antibodies against CD8a (Pacific Blue, Life Technologies, clone 5H10-1), CD19 (PE-CF594, BD Biosciences), CD44 (APC, Biolegend), CD62L (APC-Cy7, Biolegend), CD27 (PE-Cy7, Life Technologies), and 1 of 15 TCR Vβ-chains (FITC, including Vβ2, Vβ3, Vβ4, Vβ5.1/5.2, Vβ6, Vβ7, Vβ8.1/8.2, Vβ9, Vβ10b, Vβ11, Vβ12, Vβ13, Vβ14, Vβ17a, BD Pharmingen) were added and incubation continued for 20 min. Samples were then read in.

Peptide stimulation and intracellular cytokine staining

Splenocytes were isolated as described above. Suspensions were split into 11 samples and either stimulated with varying doses of respective peptides (final concentrations ranging from 10^{-6} to 10^{-14} M, peptides synthesized by and purchased from Peptides and Elephants), stimulated with PMA/Ionomycin for positive control, or just medium for negative control. Samples were incubated at 37°C for 5 h. After 1 h, 1 μL of Golgi Plug (BD Biosciences) was added to each well while keeping agitation to a minimum. After incubation, cells were washed, incubated with Fc-block (BD Bioscience), and 0.1 μg Ethidium-monazide-bromide (EMA, Molecular Probes) for 20 min under light, washed, stained with antibodies against CD8a (FITC, Biolegend) and CD19 (PE-CF594, BD Biosciences) and washed and fixed with Cytofix/Cytoperm (BD Bioscience). Samples were incubated with anti-IFN-γ (Life Technologies) for 20 min, washed, and read in. A log(agonist) versus response model (Prism 7) was fitted to the percentages of INF-γ$^+$ of CD8$^+$ of increasing peptide dose samples and logEC$_{50}$ reported as functional avidity.

xCELLigence in vitro tumor killing assay

Cells of the OVA-expressing PancOVA cell line were suspended in RPMI-1640 medium and seeded into a 96-well E-plate (OMNI Life Science), 10,000 cells per well, and placed in an RTCA MP (OMNI Life Science) inside an incubator at 37°C. The following day, splenocytes were isolated 6 days after recall infection, as

described above. Cells were resuspended in an H-2K^b/OVA$_{257\text{-}264}$ reversible multimer solution, irrespective of the inducing *L.m.* strain, for at least 45 min. CD8a (Pacific Blue, Life Technologies, clone 5H10-1) and CD19 (PE-CF594, BD Biosciences) antibodies were added after 25 min and coincubated for at least 20 min. Living, CD19$^-$, CD8$^+$, reversible OVA multimer$^+$ cells were sorted into RPMI-1640 medium, d-biotin added to remove reversible multimers and 25,000 T cells, 50,000 T cells, or just medium added to the PancOVA cells in duplicates or triplicates per sample condition. E-Plates were left at room temperature for 30 min to let T cells set, as per supplier recommendation, creating a bump in cell indices after placing the plates back in the RTCA MP. Additions were carried out ca. 24 h after initial seeding during which we assumed a doubling of PancOVA cell numbers. Cell indices were normalized to addition time points and killing capacity (cytolysis) quantified as the average difference in normalized cell index of sample wells (T cells added) to control wells (medium added) after 48 h.

In vivo tumor killing assay

Splenocytes were isolated d8 p.i. as described above. Cells were resuspended in an H-2K^b/OVA$_{257\text{-}264}$ reversible multimer solution, irrespective of the inducing *L.m.* strain, for at least 45 min. CD8a (Pacific Blue, Life Technologies, clone 5H10-1) and CD19 (PE-CF594, BD Biosciences) antibodies were added after 25 min and coincubated for at least 20 min. Living, CD19$^-$, CD8$^+$, reversible OVA multimer$^+$ cells were sorted, d-biotin was added to remove reversible multimers and 25,000 sorted cells per recipient mouse were administered intraperitoneally after irradiating recipients with 5 Gy. Controls received saline solution after irradiation. The following day, 1×10^6 OVA-expressing MC38-OVA tumor cells per recipient mouse were injected subcutaneously into the flank. Recipients were regularly surveilled and sacrificed if the tumor reached a size of ≥15 mm in any dimension. Alternatively, after a maximum of 50 days of not reaching critical tumor burden or if ulcers started to form, mice were sacrificed and censored in the analysis.

In silico k_{off}-rate analysis

Weighted means of the H-2K^b/OVA$_{257\text{-}264}$-TCR k$_{\text{off}}$-rates in Fig. 2 were calculated using the population size (in events) as weights. "Dissociation fit outputs" of sets of TCRs were generated by concatenating their dissociation data exported from FlowJo and analyzing them like a single TCR dissociation data file. The equation used for "equation predicted $t_{1/2}$" is detailed in Supporting information Fig. S1. It calculates a weighted average of the known one-phase exponential decays of all kinetics in the population, resulting in a multiphase decay curve. The same one-phase decay model was fitted to this curve to yield a single $t_{1/2}$ which was plotted as "equation predicted t$_{1/2}$." Weighting of HLA-A2/YFV NS4B$_{214\text{-}222}$ k_{off}-rates in Fig. 6 was achieved by adjusting the fre-

quency parameter in the aforementioned equation, for example, to 50%/50% in Fig. 6E, to yield the "equation predicted $t_{1/2}$." To weight kinetics for the "dissociation fit output," data from a given dissociation were inserted into the merged data file multiple times to mimic the acquisition of more events for that dissociation. For example, to weight a dissociation with 3000 events 1:1 with a dissociation with 1000 events, the data of the latter were appended three times to the FlowJo export of the former and analyzed as one dissociation.

Conflict of interest: The authors declare no financial conflict of interest.

Ethics approval statement: All animal experiments were approved by the District Government of Upper Bavaria (Department 5, Environment, Health and Consumer Protection). The local Ethical Committee's (Ethikkommission der Medizinischen Fakultät der Technischen Universität München) approval was received for the studies and the informed consent of all participating subjects was obtained (reference number 34/20S).

Author contributions: PL, KS, ED, ME, MN, and DHB conceptualized and designed the experiments. PL and MN produced MHC reagents. PH (human k_{off}-rates), SJ (k_{off}-rates of murine TCR library for H-2K^b/OVA$_{257\text{-}264}$), and PL & KLM (all other experiments) performed the experiments. AP established in vivo tumor experiment methodology. PL applied bioinformatics and statistical analysis. PL drafted the manuscript and KLM, ED, KS, and DHB revised it. All authors contributed to and approved the submitted version.

Peer review: The peer review history for this article is available at https://publons.com/publon/10.1002/eji.202149597.

Data availability statement: The data that support the findings of this study are available from the corresponding author upon reasonable request.

References

1 **van der Merwe, P. A. and Davis, S. J.**, Molecular interactions mediating T cell antigen recognition. *Annu. Rev. Immunol.* 2003. **21**: 659–684.

2 **Trambas, C. M. and Griffiths, G. M.**, Delivering the kiss of death. *Nat. Immunol.* 2003. **4**: 399–403.

3 **Zhong, S., Malecek, K., Johnson, L. A., Yu, Z., Vega-Saenz de Miera, E., Darvishian, F., McGary, K. et al.**, T-cell receptor affinity and avidity defines antitumor response and autoimmunity in T-cell immunotherapy. *Proc. Natl. Acad. Sci. USA* 2013. **110**: 6973–6978.

4 **Hombrink, P., Raz, Y., Kester, M. G. D., de Boer, R., Weißbrich, B., von dem Borne, P. A., Busch, D. H. et al.**, Mixed functional characteristics correlating with tcr-ligand koff -rate of MHC-tetramer reactive t cells within the naive T-cell repertoire. *Eur. J. Immunol.* 2013. **43**: 3038–3050.

5 **Nauerth, M., Weißbrich, B., Knall, R., Franz, T., Dössinger, G., Bet, J., Paszkiewicz, P. J.**, et al., TCR-ligand koff rate correlates with the protective capacity of antigen-specific Cd8⁺ T cells for adoptive transfer. *Sci. Transl. Med.* 2013. **5**: 192ra87.

6 **Schober, K., Voit, F., Grassmann, S., Müller, T. R., Eggert, J., Jarosch, S., Weißbrich, B. et al.**, Reverse TCR repertoire evolution toward dominant low-affinity clones during chronic CMV infection. *Nat. Immunol.* 2020. **21**: 434–441.

7 **Martinez, R. J., Andargachew, R., Martinez, H. A. and Evavold, B. D.**, Low-affinity CD4⁺ T cells are major responders in the primary immune response. *Nat. Commun.* 2016. **7**: 13848.

8 **Zehn, D., Lee, S. Y. and Bevan, M. J.**, Complete but curtailed T cell response to very low affinity antigen. *Nature* 2009. **458**: 211–214.

9 **Lever, M., Maini, P. K., van der Merwe, P. A. and Dushek, O.**, Phenotypic models of T cell activation. *Nat. Rev. Immunol.* 2014. **14**: 619–629.

10 **Kalergis, A. M., Boucheron, N., Doucey, M. A., Palmieri, E., Goyarts, E. C., Vegh, Z., Luescher, I. F. and Nathenson, S. G.**, Efficient T cell activation requires an optimal dwell-time of interaction between the TCR and the PMHC complex. *Nat. Immunol.* 2001. **2**: 229–234.

11 **Corr, M., Slanetz, A. E., Boyd, L. F., Jelonek, M. T., Khilko, S., al-Ramadi, B. K., Kim, Y. S. et al.**, T cell receptor-mhc class i peptide interactions: Affinity, kinetics, and specificity. *Science* 1994. **265**: 946–949.

12 **Huppa, J. B., Axmann, M., Mörtelmaier, M. A., Lillemeier, B. F., Newell, E. W., Brameshuber, M., Klein, L. O. et al.**, TCR-peptide-MHC interactions in situ show accelerated kinetics and increased affinity. *Nature* 2010. **463**: 963–967.

13 **Huang, J., Zarnitsyna, V. I., Liu, B., Edwards, L. J., Jiang, N., Evavold, B. D. and Zhu, C.**, The kinetics of two-dimensional TCR and PMHC interactions determine T-cell responsiveness. *Nature* 2010. **464**: 932–936.

14 **Hebeisen, M., Schmidt, J., Guillaume, P., Baumgaertner, P., Speiser, D. E., Luescher, I. and Rufer, N.**, Identification of rare high-avidity, tumor-reactive CD8⁺ T cells by monomeric TCR-ligand off-rates measurements on living cells. *Cancer Res.* 2015. **75**: 1983–1991.

15 **Dutoit, V., Rubio-Godoy, V., Doucey, M. - A., Batard, P., Liénard, D., Rimoldi, D., Speiser, D. et al.**, Functional avidity of tumor antigen-specific ctl recognition directly correlates with the stability of MHC/peptide multimer binding to TCR. *J. Immunol.* 2002. **168**: 1167–1171.

16 **Yee, C., Savage, P. A., Lee, P. P., Davis, M. M. and Greenberg, P. D.**, Isolation of high avidity melanoma-reactive CTL from heterogeneous populations using peptide-MHC tetramers. *J. Immunol.* 1999. **162**: 2227–2234.

17 **Busch, D. H. and Pamer, E. G.**, T cell affinity maturation by selective expansion during infection. *J. Exp. Med.* 1999. **189**: 701–710.

18 **Sherwood, A. M., Emerson, R. O., Scherer, D., Habermann, N., Buck, K., Staffa, J., Desmarais, C. et al.**, Tumor-infiltrating lymphocytes in colorectal tumors display a diversity of T cell receptor sequences that differ from the T cells in adjacent mucosal tissue. *Cancer Immunol. Immunother* 2013. **62**: 1453–1461.

19 **Neuenhahn, M., Albrecht, J., Odendahl, M., Schlott, F., Dössinger, G., Schiemann, M., Lakshmipathi, S. et al.**, Transfer of minimally manipulated

CMV-specific T cells from stem cell or third-party donors to treat cmv infection after allo-HSCT. *Leukemia* 2017. **31**: 2161–2171.

20 **Verfuerth, S., Peggs, K., Vyas, P., Barnett, L., O'Reilly, R. J. and Mackinnon, S.**, Longitudinal monitoring of immune reconstitution by CDR3 size spectratyping after T-cell–depleted allogeneic bone marrow transplant and the effect of donor lymphocyte infusions on T-cell repertoire. *Blood* 2000. **95**: 3990–3995.

21 **Twyman-Saint Victor, C., Rech, A. J., Maity, A., Rengan, R., Pauken, K. E., Stelekati, E., Benci, J. L. et al.**, Radiation and dual checkpoint blockade activate non-redundant immune mechanisms in cancer. *Nature* 2015. **520**: 373–377.

22 **Allard, M., Couturaud, B., Carretero-Iglesia, L., Duong, M. N., Schmidt, J., Monnot, G. C., Romero, P. et al.**, TCR-ligand dissociation rate is a robust and stable biomarker of cd8+ t cell potency. *JCI Insight* 2017. **2**: e92570.

23 **Nauerth, M., Stemberger, C., Mohr, F., Weißbrich, B., Schiemann, M., Germeroth, L. and Busch, D. H.**, Flow cytometry-based TCR-ligand koff -rate assay for fast avidity screening of even very small antigen-specific T cell populations ex vivo. *Cytometry. Part A J Int Socr Analyticl Cytol* 2016. **89**: 816–825.

24 **Gannon, P. O., Wieckowski, S., Baumgaertner, P., Hebeisen, M., Allard, M., Speiser, D. E. and Rufer, N.**, Quantitative TCR:pMHC dissociation rate assessment by ntamers reveals antimelanoma T cell repertoires enriched for high functional competence. *J. Immunol.* 2015. **195**: 356–366.

25 **Martin-Blanco, N., Blanco, R., Alda-Catalinas, C., Bovolenta, E. R., Oeste, C. L., Palmer, E., Schamel, W. W. et al.**, A window of opportunity for cooperativity in the T cell receptor. *Nat. Commun.* 2018. **9**: 2618.

26 **Fuertes Marraco, S. A., Soneson, C., Cagnon, L., Gannon, P. O., Allard, M., Abed Maillard, S., Montandon, N. et al.**, Long-lasting stem cell-like memory CD8⁺ T cells with a naïve-like profile upon yellow fever vaccination. *Sci. Transl. Med.* 2015. **7**: 282ra48.

27 **Stone, J. D., Chervin, A. S. and Kranz, D. M.**, T-cell receptor binding affinities and kinetics: Impact on t-cell activity and specificity. *Immunology* 2009. **126**: 165–176.

28 **Matsui, K., Boniface, J. J., Steffner, P., Reay, P. A. and Davis, M. M.**, Kinetics of T-cell receptor binding to peptide/i-ek complexes: correlation of the dissociation rate with T-cell responsiveness. *Proc. Natl. Acad. Sci. USA*. 1994. **91**: 12862–12866.

29 **Bullock, T. N., Mullins, D. W., Colella, T. A. and Engelhard, V. H.**, Manipulation of avidity to improve effectiveness of adoptively transferred CD8(+) T cells for melanoma immunotherapy in human MHC class i-transgenic mice. *J. Immunol.* 2001. **167**: 5824–5831.

30 **Wilde, S., Sommermeyer, D., Leisegang, M., Frankenberger, B., Mosetter, B., Uckert, W. and Schendel, D. J.**, Human antitumor CD8⁺ T cells producing Th1 polycytokines show superior antigen sensitivity and tumor recognition. *J. Immunol.* 2012. **189**: 598–605.

31 **Tian, S., Maile, R., Collins, E. J. and Frelinger, J. A.**, Cd8+ T cell activation is governed by TCR-peptide/MHC affinity, not dissociation rate. *J. Immunol.* 2007. **179**: 2952–2960.

32 **Laugel, B., van den Berg, H. A., Gostick, E., Cole, D. K., Wooldridge, L., Boulter, J., Milicic, A. et al.**, Different t cell receptor affinity thresholds and CD8 coreceptor dependence govern cytotoxic t lymphocyte activation and tetramer binding properties. *J. Biol. Chem.* 2007. **282**: 23799–23810.

33 **Rius, C., Attaf, M., Tungatt, K., Bianchi, V., Legut, M., Bovay, A., Donia, M. et al.**, Peptide-MHC class i tetramers can fail to detect relevant functional T cell clonotypes and underestimate antigen-reactive T-cell populations. *J. Immunol.* 2018. **200**: 2263–2279.

34 **Savage, P. A., Boniface, J. J. and Davis, M. M.**, A kinetic basis for T cell receptor repertoire selection during an immune response. *Immunity*. 1999. **10**: 485–492.

35 **Schmid, D. A., Irving, M. B., Posevitz, V., Hebeisen, M., Posevitz-Fejfar, A., Sarria, J.-C. F., Gomez-Eerland, R. et al.**, Evidence for a TCR affinity threshold delimiting maximal Cd8 T cell function. *J. Immunol.* 2010. **184**: 4936–4946.

36 **Tan, M. P., Gerry, A. B., Brewer, J. E., Melchiori, L., Bridgeman, J. S., Bennett, A. D., Pumphrey, N. J. et al.**, T cell receptor binding affinity governs the functional profile of cancer-specific Cd8$^+$ T cells. *Clin. Exp. Immunol.* 2015. **180**: 255–270.

37 **Cafri, G., Yossef, R., Pasetto, A., Deniger, D. C., Lu, Y. - C., Parkhurst, M., Gartner, J. J. et al.**, Memory T cells targeting oncogenic mutations detected in peripheral blood of epithelial cancer patients. *Nat. Commun.* 2019. **10**: 449.

38 **D'Ippolito, E., Schober, K., Nauerth, M. and Busch, D. H.**, T cell engineering for adoptive T cell therapy: safety and receptor avidity. *Cancer Immunol. Immunother.* 2019. **68**: 1701–1712.

39 **Cossarizza, A., Chang, H. - D., Radbruch, A., Abrignani, S., Addo, R., Akdis, M., Andrä, I. et al.**, Guidelines for the use of flow cytometry and cell sorting in immunological studies (third edition). *Eur. J. Immunol.* 2021. **51**: 2708–3145.

Full correspondence: Dr. Kilian Schober and Dirk H. Busch, Institute for Medical Microbiology, Immunology and Hygiene, Technische Universität München (TUM), Munich, Germany.
e-mail: Kilian.Schober@uk-erlangen.de; dirk.busch@tum.de